Fast Fourier nonlinear vibration analysis

A. Cardona, A. Lerusse, M. Géradin

Abstract We present an implementation of the multi-harmonic balance method (MHB) where intensive use of the Fast Fourier Transform algorithm (FFT) is made at all stages of calculations. The MHB method is not modified in essence, but computations are organized to obtain a very attractive method that can be applied systematically on general nonlinear vibration problems. The resulting non-linear algebraic problem is solved by a particular implementation of a continuation method. Nonlinear vibration results are analyzed a posteriori by a Floquet method to determine their stability. The technique is applied on a series of problems of different nature, demonstrating the robustness and flexibility of the approach.

1
Introduction

The multi-harmonic balance method (MHB) has been widely used to solve nonlinear vibration problems under periodic excitation. It finds applications in several fields of mechanical engineering, e.g. machine dynamics, vehicle dynamics, helicopter rotor blade analysis, structural dynamics.

The method is well-known from literature. Urabe [1] investigated the convergence conditions of the method and presented numerical applications [2] using the classical Fourier transform. Lau et al. [3–5] and more recently [6] developed an incremental form of the method. Pierre et al. [7, 8] and Ferri [9] followed the same approach to solve nonlinear vibration problems involving dry-friction. Ling and Wu [10] introduced the use of the Fast Fourier Transform (FFT) algorithm in Urabe's formulation. The same path was followed by other authors [11–16].

The use of FFT permits an overwhelming gain of CPU time when computing the Fourier transform. Most authors use the FFT to switch displacements, velocities, accelerations and forces between the time and frequency domains. However, even if the original proposal by Urabe included the analytical expression of the Jacobian of the nonlinear algebraic problem, most of them avoid computing this matrix. Ling and Wu [10] used a Broyden method; Cameron and Griffin [11] used either a Picard iteration or a Jacobian matrix evaluated by finite differences; Lewandowski [14] gave particular expressions for the contributions of nonlinear terms to the Jacobian for the case of geometric nonlinearities in the form of trigonometric expansions.

In reference [15] we presented an approach which differs from most others in that an analytical expression for the Jacobian matrix of the nonlinear algebraic problem is developed for general applications. This fact allows to solve the nonlinear algebraic problem with utmost efficiency, reaching quadratic convergence rate. We have shown how the Jacobian matrix can be computed from the Fourier transform of the time domain stiffness, damping and mass matrices of the system under analysis.

The MHB leads to a nonlinear algebraic problem in which the solution should be searched in the Fourier transformed displacements versus excitation period space. The solution is found in the form of a nonlinear dynamic equilibrium path in this space for varying values of the excitation period. Standard Newton iteration fails to find a solution in the vicinity of singular points on the nonlinear dynamic path. In order to solve this problem, Lewandowski [14] used a continuation method in which the solution is searched in an enlarged parameter space, following a strategy proposed by Crisfield and widely used in structural mechanics [17, 18]. In this paper, we use the same approach, extending it to general nonlinear vibration problems. To this end, we develop general expressions of the derivative of the transformed residue with respect to the period of analysis which are computed by using the FFT.

We investigate next the stability of solutions by a Floquet method. We discuss two different approximations for evaluating numerically the monodromy matrix. The first one follows an idea by Hsu [19, 20] in which a step wise variation of the system matrix is assumed and the state matrix integration is done by computing matrix exponentials. The second approach is based on using the Newmark time integration scheme for integration of the state transition matrix. Particular aspects concerning the numerical problems encountered and how to solve them are discussed in section 4.

Finally, several application examples are presented. The first one concerns the Duffing equation which is solved for

---

A. Cardona
Grupo de Tecnologiá Mecánica – INTEC,
Universidad del Litoral – Conicet,
Güemes 3450, 3000 Santa Fe, Argentina

A. Lerusse
Dynamique des Constructions Mécaniques – LTAS,
Université de Liège, rue E. Solvay 21, B4000 Liège, Belgium

M. Géradin
Structural Mechanics Unit, JRC, I-21020 Ispra, Italy

a wide range of values of the nonlinear cubic term. The second example is an application of the technique to compute nonlinear vibrations of a clamped beam with a dry-friction damper. Results are compared to those of an experimental setup. The third and final example concerns the computation of nonlinear vibrations in a shallow hanging cable excited by a moving support. This last example is representative of cable vibrations in cable stayed bridges and in electric power transmission lines [21].

2
The multi-harmonic balance method

The multi-harmonic balance method can be applied to autonomous and non-autonomous dynamic systems with different types of nonlinearities (large displacements, dry friction, contact, ...). We develop hereafter the formulation for non-autonomous dynamic systems, the autonomous case requiring a slight modification to impose the vibration amplitude. The objective is to obtain a solution $\mathbf{q}(t)$ to the nonlinear dynamics problem

$$\mathbf{M}\ddot{\mathbf{q}} + \mathbf{g}_{nl}(\mathbf{q}, \dot{\mathbf{q}}) = \mathbf{f}(t) \tag{1}$$

under periodic loading $\mathbf{f}(t)$, where $\mathbf{g}_{nl}$ is the nonlinear forces vector of the dynamic system and $\mathbf{f}$ is the periodic excitation such that $\mathbf{f}(t + T_f) = \mathbf{f}(t)$, with T_f the period of excitation.

The proposed method to solve problem (1) consists of alternating between time and frequency domains, taking advantage in this manner of the ease to evaluate nonlinearities in the time domain while capturing periodic motion in the frequency domain. The solution $\mathbf{q}$ is sampled at N instants and assumed periodic,

$$\mathbf{q}_k = \mathbf{q}(k\Delta t) \qquad k = 0, \ldots, N - 1 \tag{2}$$

with $\Delta t = h = T/N$. Here, $T = np \times T_f$ is the period of analysis; it is selected to be several (np) times the period of excitation to allow the search of sub-harmonics in the response.

Since $\mathbf{q}$ is sampled at N instants, it can be expressed in terms of at most N Fourier components

$$\mathbf{q}_k = \frac{1}{\sqrt{2N}} \left(\hat{\mathbf{q}}_{0,0} + 2 \sum_{n=1}^{N/2-1} (C_{kn,0}\hat{\mathbf{q}}_{n,0} + C_{kn,1}\hat{\mathbf{q}}_{n,1}) \right. $$
$$\left. + (-1)^k \hat{\mathbf{q}}_{N/2,0} \right) \tag{3}$$

The Fourier components of displacement $\hat{\mathbf{q}}_{n,m}$ correspond to the n-th term of the series with phase m; the coefficients $C_{kn,m}$ are defined as

$$C_{kn,m} = \cos\left(\frac{2\pi n}{T} t_k - m\frac{\pi}{2} \right) \tag{4}$$

the phase number m being either 0 or 1, denoting respectively the cosine and sine terms.

Equation (3) is nothing else than the inverse Fourier transform of $\hat{\mathbf{q}}_{n,m}$. We note it in the concise form

$$\mathbf{q}_k = \mathrm{ift}_k^{n,m}(\hat{\mathbf{q}}_{n,m}) \tag{5}$$

Clearly, this form of expressing the Fourier series is intended for implementation by the Fast Fourier Transform algorithm [22].

The number of harmonics required to obtain satisfactory approximation to the solution depends on the frequency and on the amplitude of the excitation but is generally much lower than N. Therefore we can truncate the Fourier expansion to N_H harmonics

$$\mathbf{q}_k = \sqrt{\frac{2}{N}} \left(\frac{1}{2}\hat{\mathbf{q}}_{0,0} + \sum_{n=1}^{N_H} \sum_{m=0}^{1} C_{kn,m}\hat{\mathbf{q}}_{n,m} \right) \tag{6}$$

$N_H < N/2 - 1$ being the number of harmonics retained in the expansion.

Velocities and accelerations are computed through time-differentiation of equations (6)

$$\dot{\mathbf{q}}_k = \sqrt{\frac{2}{N}} \frac{2\pi}{T} \sum_{n=1}^{N_H} n(-C_{kn,1}\hat{\mathbf{q}}_{n,0} + C_{kn,0}\hat{\mathbf{q}}_{n,1})$$

$$\ddot{\mathbf{q}}_k = -\sqrt{\frac{2}{N}} \left(\frac{2\pi}{T}\right)^2 \sum_{n=1}^{N_H} n^2(C_{kn,0}\hat{\mathbf{q}}_{n,0} + C_{kn,1}\hat{\mathbf{q}}_{n,1}) \ . \tag{7}$$

2.1
Fourier Galerkin dynamic solution

The local solution to the nonlinear dynamic problem (1) is such that the residue $\mathbf{r}_k$ is annihilated at any time instant t_k

$$\mathbf{r}_k = \mathbf{r}(t_k) = \mathbf{M}\ddot{\mathbf{q}}_k + \mathbf{g}_{nl}(\mathbf{q}_k, \dot{\mathbf{q}}_k) - \mathbf{f}_k = 0$$
$$k = 0, 1, \ldots, N - 1 \ , \tag{8}$$

Instead of verifying the strong form of equilibrium (8), let us require to verify the following averaged form of dynamic equilibrium

$$\hat{\mathbf{r}}_{l,m}$$

$$= \begin{cases} \frac{1}{2}\sqrt{\frac{2}{N}} \sum_{k=0}^{N-1} C_{kl,0}(\mathbf{M}\ddot{\mathbf{q}}_k + \mathbf{g}_{nl} - \mathbf{f}_k) = 0 & \begin{array}{l} l = 0 \\ m = 0 \end{array} \\ \sqrt{\frac{2}{N}} \sum_{k=0}^{N-1} C_{kl,m}(\mathbf{M}\ddot{\mathbf{q}}_k + \mathbf{g}_{nl} - \mathbf{f}_k) = 0 & \begin{array}{l} l = 1, 2, \ldots, N_H \\ m = 0, 1 \end{array} \end{cases} \tag{9}$$

Note that there are only $2 \times N_H + 1$ values $\hat{\mathbf{r}}_{l,m}$ since $\hat{\mathbf{r}}_{0,1} = 0$. Equation (9) is almost the direct Fourier transform of $\mathbf{r}_k$ (truncated to N_H harmonics). It differs only by the term $\hat{\mathbf{r}}_{0,0}$ which is affected by a coefficient of one half to obtain a symmetric tangent matrix (see later). From now on, we refer to $\hat{\mathbf{r}}_{l,m}$ as the Fourier transform of $\mathbf{r}_k$, but keeping in mind the particular expression (9). We note it in the following compact form

$$\hat{\mathbf{r}}_{l,m} = \mathrm{ft}_{l,m}^k(\mathbf{r}_k) \tag{10}$$

Actually, the latter equation can be seen as a system of $2 \times N_H + 1$ nonlinear algebraic equations with $2 \times N_H + 1$ unknowns $\hat{\mathbf{q}}_{l,m}$. The following diagram describes the relations existing between the considered entities

$$\begin{array}{ccc} \mathbf{q}_k, \dot{\mathbf{q}}_k, \ddot{\mathbf{q}}_k & \xleftarrow{\text{eqns (6, 7)}} & \hat{\mathbf{q}}_{l,m} \\ \downarrow \mathbf{r}() & & \downarrow \hat{\mathbf{r}}() \\ \mathbf{r}_k & \xrightarrow{\quad \mathrm{ft}_{l,m}^k \quad} & \hat{\mathbf{r}}_{l,m} \end{array} \tag{11}$$

It illustrates the process of switching between frequency and time domains to compute the solution. The residual vector can then be written in the form

$$\mathbf{r}_{l,m} = \mathrm{ft}_{l,m}^{k}(\mathbf{r}(\mathbf{q}_k, \dot{\mathbf{q}}_k, \ddot{\mathbf{q}}_k(\hat{\mathbf{q}}_{ns}))) \tag{12}$$

This system of nonlinear algebraic equations will be solved using an appropriate method of solution (see next section). A solution of Newton type requires computing the Jacobian matrix

$$S = \left[\frac{\partial \hat{\mathbf{r}}_{l,m}}{\partial \hat{\mathbf{q}}_{n,s}}\right] \tag{13}$$

Let us denote by $\mathbf{K}_k$ the tangent stiffness (derivative of the nonlinear force $\mathbf{r}$) evaluated at $\mathbf{q}_k$

$$\mathbf{K}_k = \frac{\partial \mathbf{r}}{\partial \mathbf{q}}(\mathbf{q}_k, \dot{\mathbf{q}}_k) = \frac{\partial \mathbf{g}_{\mathrm{nl}}}{\partial \mathbf{q}}(\mathbf{q}_k, \dot{\mathbf{q}}_k) \tag{14}$$

and $\widehat{\mathbf{K}}_{l,m}$ its Fourier transform

$$\widehat{\mathbf{K}}_{l,m} = \mathrm{ft}_{l,m}^{k}(\mathbf{K}_k) \tag{15}$$

It can then be shown that the coefficient matrix S is formed of three contributions

$$S = S_{\mathbf{q}} + S_{\dot{\mathbf{q}}} + S_{\ddot{\mathbf{q}}} \tag{16}$$

where $S_{\mathbf{q}}$ is the contribution arising from stiffness, $S_{\dot{\mathbf{q}}}$ is the contribution from damping and $S_{\ddot{\mathbf{q}}}$ is the contribution from inertia. Their analytic expressions are given in terms of the Fourier transform of the corresponding (time domain) matrices

$$S_{\mathbf{q}} = \frac{1}{\sqrt{2N}}$$

$$\times \begin{bmatrix} \frac{1}{2}\widehat{\mathbf{K}}_{0,0} & \cdots & \widehat{\mathbf{K}}_{n,0} & \widehat{\mathbf{K}}_{n,1} \\ \vdots & \ddots & & \vdots \\ \widehat{\mathbf{K}}_{l,0} & & \widehat{\mathbf{K}}_{l+n,0} + \widehat{\mathbf{K}}_{l-n,0} & \widehat{\mathbf{K}}_{l+n,1} - \widehat{\mathbf{K}}_{l-n,1} \\ \widehat{\mathbf{K}}_{l,1} & \cdots & \widehat{\mathbf{K}}_{l-n,1} + \widehat{\mathbf{K}}_{l+n,1} & \widehat{\mathbf{K}}_{l-n,0} - \widehat{\mathbf{K}}_{l+n,0} \end{bmatrix}$$

$$S_{\dot{\mathbf{q}}} = \frac{2\pi}{T\sqrt{2N}}$$

$$\times \begin{bmatrix} 0 & \cdots & -n\widehat{\mathbf{C}}_{n,1} & n\widehat{\mathbf{C}}_{n,0} \\ \vdots & \ddots & & \vdots \\ 0 & & n(\widehat{\mathbf{C}}_{l-n,1} - \widehat{\mathbf{C}}_{l+n,1}) & n(\widehat{\mathbf{C}}_{l+n,0} + \widehat{\mathbf{C}}_{l-n,0}) \\ 0 & \cdots & n(\widehat{\mathbf{C}}_{l+n,0} - \widehat{\mathbf{C}}_{l-n,0}) & n(\widehat{\mathbf{C}}h_{l-n,1} + \widehat{\mathbf{C}}_{l+n,1}) \end{bmatrix}$$

$$S_{\ddot{\mathbf{q}}} = -\frac{4\pi^2}{T^2}\mathbf{M} \begin{bmatrix} 0 & \cdots & 0 & 0 \\ \vdots & \ddots & & \vdots \\ 0 & & \delta_{\ln}n^2\mathbf{I} & 0 \\ 0 & \cdots & 0 & \delta_{\ln}n^2\mathbf{I} \end{bmatrix}$$

$$l, n = 1, \ldots, N_H \tag{17}$$

with $\widehat{\mathbf{C}}_{l,m} = \mathrm{ft}_{l,m}^{k}(\mathbf{C}_k)$ and $\mathbf{C}_k = \partial \mathbf{g}_{\mathrm{nl}}/\partial \dot{\mathbf{q}}(\mathbf{q}_k, \dot{\mathbf{q}}_k)$. We have assumed that the mass matrix is constant, but the formulation can be easily generalized to account for nonlinear inertia terms as occurring in systems described in a non-inertial frame.

We remark that the exact analytic expression for the Jacobian matrix allows us to implement a very efficient method for solving the resulting nonlinear algebraic problem, reaching quadratic convergence rate.

3
Continuation methods for multiharmonic balance analysis

The system of nonlinear algebraic equations (12) should be solved for a wide range of analysis periods. This problem can be referred to as that of tracing the nonlinear dynamic equilibrium path of the system. Usually, the standard Newton's method is not able to converge for the full range of parameter values, so that continuation methods have to be used to progress on the equilibrium path with controlled convergence. Basically, these methods consist of enlarging the set of unknowns of the problem while adding constraints that remove the singularities that affect convergence [17, 23, 24, 18].

The nonlinear equilibrium problem to be solved can be written

$$\hat{\mathbf{r}}(\hat{\mathbf{q}}, T) = 0 \tag{18}$$

for varying values of the period of analysis T. The Newton scheme breaks down whenever $S = \partial \hat{\mathbf{r}}/\partial \hat{\mathbf{q}}$ is singular, a condition that is very easily attained in practice. To circumvent this drawback, the following homotopy is usually employed.

Let $\mathbf{h}: \mathbb{R} \to \mathbb{R}^{n+1}$ be defined by

$$\mathbf{h}(s) = \hat{\mathbf{r}}(\hat{\mathbf{q}}(s), T(s)) = 0 \tag{19}$$

$$\|(\hat{\mathbf{q}}', T')\| = 1 \tag{20}$$

where s is the new homotopy parameter, $\hat{\mathbf{q}}' = \partial \hat{\mathbf{q}}/\partial s$, $T' = \partial T/\partial s$ and $\| \cdot \|$ is an adequate norm in $\mathbb{R}^{n+1}$ (in this work we use the ℓ_2 norm, although in many situations weighted norms have been used with success [18]). Differentiating (19) we get

$$S\hat{\mathbf{q}}' + \nabla_T \mathbf{r} T' = 0 \tag{21}$$

Parameter s has a direct geometrical interpretation: it is the arc-length of the equilibrium path in the metric induced by the selected norm.

We assume in the following that the equilibrium curve, when parameterized with s, does not have any singular point. This means that each point is associated with only one unit tangent vector (thus precluding points of bifurcation of solutions). This is a rather restrictive assumption, however. Enhanced continuation algorithms have been proposed to analyze bifurcation, but they are out of the scope of this presentation (see e.g. [25]).

In order to advance along the solution path, we use the predictor–corrector scheme described in the next section.

3.1
Predictor step

By applying a forward-Euler (explicit) scheme to (20–21) to advance the solution along the equilibrium curve by a distance Δs, we obtain a first iterate $(\Delta \hat{\mathbf{q}}^{k,0}, \Delta T^{k,0})$

$$[S \; \nabla_T \hat{\mathbf{r}}]\begin{Bmatrix} \Delta \hat{\mathbf{q}}^{k,0} \\ \Delta T^{k,0} \end{Bmatrix} = 0, \quad \|(\Delta \hat{\mathbf{q}}^{k,0}, \Delta T^{k,0})\| = \Delta s \tag{22}$$

where Δs is a generalized distance in the Fourier components/period space, and where

$$\hat{q}^{k,1} = \hat{q}^{k-1} + \Delta\hat{q}^{k,0}, \qquad T^{k,1} = T^{k-1} + \Delta T^{k,0} \qquad (23)$$

The solution of the nonlinear system of equations (22) is computed in a two-stage procedure (see the bordering algorithm proposed by Keller [26]):

1. Computation of a search direction $(w, 1)$

$$Sw = -\nabla_T \hat{r} \qquad (24)$$

2. Computation of the effective predictor step

$$\Delta T^{k,0} = \pm \Delta s / \|(w, 1)\| \qquad (25)$$

$$\Delta\hat{q}^{k,0} = \Delta T^{k,0}\, w \qquad (26)$$

Note that the system (22) has two possible solutions: $(\Delta\hat{q}, \Delta T)$ and $(-\Delta\hat{q}, -\Delta T)$. The sign of the predictor step $(\Delta\hat{q}^{k,0}, \Delta T^{k,0})$ is selected such that the inner product

$$\Delta\hat{q}^{k,0} \cdot \Delta\hat{q}^{k-1} > 0 \qquad (27)$$

where $\Delta\hat{q}^{k-1}$ is the total increment of the previously converged predictor–corrector step.

3.2
Corrector step

Generally, we will get a nonzero residue after the prediction phase (unless the problem is linear), i.e.:
$\hat{r}(\hat{q}^{k,1}, T^{k,1}) \neq 0$. To return to the equilibrium path, an iterative scheme is applied starting from this point. If we adopt a Newton method, the correction equations are

$$[S \ \nabla_T \hat{r}]\begin{Bmatrix} \delta\hat{q}^m \\ \delta T^m \end{Bmatrix} = -\hat{r}(\hat{q}^{k,m-1}, T^{k,m-1}) \ . \qquad (28)$$

The total increment at iteration m results:

$$\Delta\hat{q}^{k,m} = \Delta\hat{q}^{k,m-1} + \delta\hat{q}^m \qquad (29)$$

$$\Delta T^{k,m} = \Delta T^{k,m-1} + \delta T^m \qquad (30)$$

Note that the Jacobian in (28) is a $n \times (n+1)$ matrix. Thus, we need to impose a restriction to determine uniquely the correction vector $(\delta\hat{q}^m, \delta T^m)$. The scheme proposed by Crisfield is used to this purpose. It consists of imposing to the sequence $\{(\hat{q}^{k,i}, T^{k,i}), i = 1, \ldots\}$ to rest on an hypersphere of radius Δs with center at point $(\hat{q}^{k-1}, T^{k-1})$, i.e. at the previously converged point.
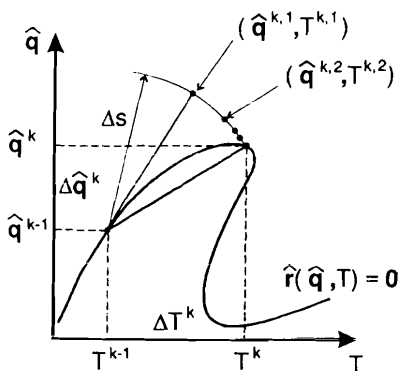

Fig. 1. Constraint description

Therefore, in order to determine the increment $(\delta\hat{q}^m, \delta T^m)$ we have to solve the quadratic equation

$$\|(\Delta\hat{q}^{k,m}, \Delta T^{k,m})\| = \Delta s \qquad (31)$$

The nonlinear system of equations (28, 31) is solved using the bordering algorithm.

To this end, let us define $v, w \in \mathbb{R}^n$ such that

$$Sv = -\hat{r} \qquad (32)$$

$$Sw = -\nabla_T \hat{r} \qquad (33)$$

where S, $\hat{r}$, $\nabla_T \hat{r}$ are evaluated at $(\hat{q}^{k,m-1}, T^{k,m-1})$. From (28), the iteration increment can be written in terms of v, w

$$(\delta\hat{q}^m, \delta T^m) = (v + \delta T^m w, \delta T^m) \qquad (34)$$

and after replacing into the quadratic restriction (31), we get

$$a\,(\delta T^m)^2 + 2b\,\delta T^m + c = 0 \qquad (35)$$

where

$$a = w^T w + 1 \qquad (36)$$

$$b = (\Delta\hat{q}^{k,m-1} + v)^T w + \Delta T^{k,m-1} \qquad (37)$$

$$c = (2\Delta\hat{q}^{k,m-1} + v)^T v \qquad (38)$$

System (28, 31) has two solutions, denoted $(\Delta\hat{q}^1, \Delta T^1)$ and $(\Delta\hat{q}^2, \Delta T^2)$, corresponding to the two roots of (35). An appropriate criterion is used to determine which solution is the most convenient one (see Crisfield [27]).

3.3
Derivative of the transformed residue with respect to the period of analysis

In order to implement the continuation method, we need computing the partial derivative of the transformed residue with respect to the period of analysis, computed keeping the Fourier components $\hat{q}_{l,m}$ fixed (i.e. term $\frac{\partial \hat{r}_{l,m}}{\partial T}$ in equation (28)). To calculate this vector, let us first note from (6, 7) that

$$\frac{\partial q_k}{\partial T} = 0 \qquad \frac{\partial \dot{q}_k}{\partial T} = -\frac{\dot{q}_k}{T} \qquad \frac{\partial \ddot{q}_k}{\partial T} = -\frac{2\ddot{q}_k}{T} \qquad (39)$$

After replacing the latter into equation (8) we get

$$\frac{\partial r_k}{\partial T} = \frac{-2M\ddot{q}_k - C_k\dot{q}_k}{T} \qquad (40)$$

Finally, from (9) we see that the Fourier transform of this vector provides the desired result

$$\frac{\partial \hat{r}_{l,m}}{\partial T} = ft_{l,m}^k\left(\frac{\partial r_k}{\partial T}\right) \ . \qquad (41)$$

3.4
Special features and remarks

At each step, the value of the hypersphere radius Δs is adapted according to the number of iterations per step prescribed by the user

$$\Delta s^k = \Delta s^{k-1} \sqrt{\frac{N_{it}^*}{N_{it}^{k-1}}} \qquad (42)$$

where N_{it}^{k-1} is the number of iterations required for convergence at the previous increment and N_{it}^* is the target number of iterations set by the user. The target number of iterations N_{it}^* controls indirectly the actual arc-length used in computations. Usually, this value is set to three or four iterations per step to trace correctly the nonlinear dynamic path without missing any important characteristics. However, an optimal selection of this parameter is somehow problem dependent.

During computations, it may happen that ΔT takes values which are not acceptable, leading to negative excitation frequencies. In this case, we do not perform the update: we reject the step and restart with a smaller value of increment Δs.

One further restriction is applied to the arc-length increment: whenever the tangent to the nonlinear dynamic path becomes close to horizontal, the arc-length increment is limited to $\frac{1}{10}$ of the analysis period in order to avoid computing excessively large predictions.

4
Solution stability analysis

Let us suppose that a periodic solution $\mathbf{q}(t)$ to the system of equations (1) has been obtained and let us now investigate its stability. This can be achieved by making use of Floquet's theory.

Let $\mathbf{y}(t)$ be a perturbation to the periodic solution $\mathbf{q}(t)$ such that actual motion is given by

$$\begin{aligned}
\mathbf{q}(t) &\longrightarrow \mathbf{q}(t) + \mathbf{y}(t) \\
\dot{\mathbf{q}}(t) &\longrightarrow \dot{\mathbf{q}}(t) + \dot{\mathbf{y}}(t) \\
\ddot{\mathbf{q}}(t) &\longrightarrow \ddot{\mathbf{q}}(t) + \ddot{\mathbf{y}}(t)
\end{aligned} \tag{43}$$

After replacing the expressions for perturbed motion into the dynamic equilibrium equation (1) and by linearizing with respect to the perturbation $\mathbf{y}(t)$ we get

$$\mathbf{M}\ddot{\mathbf{y}} + \mathbf{C}(t)\dot{\mathbf{y}} + \mathbf{K}(t)\mathbf{y} = \mathbf{0} \tag{44}$$

with the time-dependent tangent stiffness and damping matrices $\mathbf{K}(t)$ and $\mathbf{C}(t)$. We can express this second order system as a $2n$-first order system

$$\dot{\mathbf{x}} = \mathbf{A}(t)\mathbf{x} \tag{45}$$

where

$$\mathbf{A}(t) = \begin{bmatrix} \mathbf{0} & \mathbf{1} \\ -\mathbf{M}^{-1}\mathbf{K} & -\mathbf{M}^{-1}\mathbf{C} \end{bmatrix} \quad \mathbf{x} = \begin{bmatrix} \mathbf{y} \\ \dot{\mathbf{y}} \end{bmatrix} \tag{46}$$

where $\dot{\mathbf{x}}$ denotes the derivative of the $2n$-state vector $\mathbf{x}$ with respect to t, and where matrix $\mathbf{A}(t)$ is periodic, i.e. $\mathbf{A}(t) = \mathbf{A}(t+T)$. Equation (45) constitutes an homogeneous linear parametrically-excited system described in state equation form.

Let $\phi_j(t), j = 1, 2n$ be the solutions to the $2n$ linear systems

$$\dot{\phi}_j(t) = \mathbf{A}(t)\phi_j(t) \qquad \phi_j(t_0) = \mathbf{e}_j \tag{47}$$

where $\mathbf{e}_j$ is the j-th canonical basis vector in $\mathbb{R}^{2n}$. The time varying-solutions $\phi_j(t)$ are grouped to form the state transition matrix

$$\mathbf{\Phi}(t, t_0) = [\phi_1(t) \ \phi_2(t) \ \dots \ \phi_{2n}(t)] \tag{48}$$

where the second argument denotes the dependence on initial time. $\mathbf{\Phi}(t, t_0)$ forms a fundamental system if the determinant

$$\phi(t) = \det(\mathbf{\Phi}(t, t_0)) \neq 0 \tag{49}$$

is different from zero everywhere in the time interval of interest. In such case, the general homogeneous solution of equation (45) can be constructed from the $2n$ linear independent solutions $\phi_j(t)$.

The monodromy matrix is defined as the state transition matrix at the end of one analysis period

$$\mathbf{B} = \mathbf{\Phi}(T, 0) \tag{50}$$

This nonsingular matrix plays the main role in stability investigation of periodic systems. Its eigenvalues, solutions of the characteristic equation

$$\det(\mathbf{B} - \mu\mathbf{I}) = 0 \tag{51}$$

are generally complex. They are denoted the characteristic multipliers μ of the system in terms of which the stability statements of linear parametrically-excited systems can be formulated.

Stable periodic solutions of equation (1) are characterized by a solution $\mathbf{x} = \mathbf{0}$ to the linearized equation (45). Then, the following conditions can be obtained from equation (51):

The solution $\mathbf{x} = \mathbf{0}$ of a linear system 45) of first order differential equations with periodic system matrix $\mathbf{A}(t)$ is

1. asymptotically stable if all characteristic multipliers are such that $|\mu_j| < 1, j = 1, \dots, 2n$,
2. stable in Lyapunov sense if $|\mu_j| \leq 1, j = 1, \dots, 2n$, and at least one $|\mu_k| = 1$ with $d_k = v_k$,
3. unstable if $|\mu_k| > 1$ or $|\mu_k| = 1$, with $d_k < v_k$ for at least one $k, k \in [1, 2n]$,

where d_k and v_k characterize respectively the defect and the multiplicity of the eigenvalue μ_k.

4.1
Numerical evaluation of the monodromy matrix

The key aspect of the Floquet method is the computation of the monodromy matrix $\mathbf{B}$. It can be numerically determined in different ways. For example, a high order Runge–Kutta approach with $2n$ integrations of equation (47) over the time interval $[0, T]$ has been used in [28]. In this work, we have tested two methods [29] to evaluate $\mathbf{B}$. Our first approach has been based on the work by P. Friedmann et al. [19, 20] in terms of an assumed stepwise variation of the state transition matrix and integration by matrix exponentiation. The second approach we have followed is based on the Newmark time integration scheme.

4.1.1
Evaluation of the monodromy matrix through matrix exponentiation

Let us assume that the linear system (45) is time invariant (zero-hold approximation) between time instants t_k and t_{k+1}, and that matrix $\mathbf{A}$ is thus constant on this interval. Between these two time instants one can write

$$x_{k+1} = \exp(hA_k)x_k \qquad (52)$$

where A_k is the system matrix between times t_k and t_{k+1} and $h = t_{k+1} - t_k$ is the time-step length.

The monodromy matrix is then computed as the product of the individual transition matrices. This assembling phase is performed over one cycle of the response

$$x_{N+1} = \underbrace{\prod_{k=1}^{N} \exp(hA_k)}_{B} \, x_1 = Bx_1 \qquad (53)$$

The multiplication ordering sequence is such that the k-th factor must be premultiplied by the $(k+1)$-th one; N is the number of time steps over one analysis cycle.

The spectral radius of the monodromy matrix B characterizes the stability of the periodic solution. The only assumption made so far is that the system is considered constant between two consecutive time steps. This is a weak assumption because of the large number of time steps used by the multi-harmonic method. Two numerical difficulties are raised by this approach: the evaluation of the matrix exponential and the matrix multiplication during the assembly phase. Both aspects are discussed hereafter.

4.1.1.1
Computation of the matrix exponential
Let us compute the matrix exponential by an L-th order truncated Taylor series

$$\exp(hA_k) = \sum_{j=0}^{\infty} \frac{(hA_k)^j}{j!} \simeq \sum_{j=0}^{L} \frac{(hA_k)^j}{j!} \qquad (54)$$

This is one of the many methods that have been proposed in the literature to evaluate the exponential of a matrix (see for instance [30]). We have made also some experiments using Padé approximants (in fact, (54) is a particular Padé approximant) but the truncated power series performs better in the present context and therefore we retain this algorithm.

The matrix exponential can be adequately approximated by a truncated power series around zero provided that the norm of matrix hA_k remains small compared to 1. In order to remain within the domain of convergence of the power series, matrix hA_k is scaled by computing an integer a and a matrix $\overline{A}$ verifying the relationship

$$hA_k = 2^a \overline{A} \qquad (55)$$

with

$$\|\overline{A}\|_\infty \leq \tfrac{1}{2} \qquad (56)$$

We can then write

$$\exp(hA_k) = \exp(2^a \overline{A}) = \left(\exp(\overline{A})\right)^{2^a} \qquad (57)$$

Therefore, in order to evaluate accurately $\exp(hA_k)$ we first compute $\exp(\overline{A})$ by the truncated power series (54) and then perform a successive matrix–matrix products.

The relative error of this method for computing the exponential of a matrix is bounded by [31]

$$\epsilon_{rel} \leq \frac{2^{2+a-L}}{(L+1)!} \exp\left(\frac{2^{2+a-L}}{(L+1)!}\right) \qquad (58)$$

giving us a means to adjust L by specifying a required relative accuracy. For instance, if $a = 3$ and $L = 6$, we get 4-digit accuracy when evaluating the matrix exponential in this way.

4.1.1.2
Computation of the product of exponentials
After having computed $\exp(hA_k)$, $k = 1, \ldots, N$, the monodromy matrix is obtained by making the product of all the factors as indicated in (53). However, even if the final monodromy matrix B has small components, the partial products can be very large in magnitude, leading to partial product overflow.

To avoid it, we compute successive scale factors α_k such that the matrix obtained after each sub-product has an infinity norm set equal to 1. The scale factors α_k are meanwhile stored in logarithm form, resulting in the following recursive procedure to compute B: starting from

$C_0 = I$, compute

$$\left. \begin{aligned} C_k^* &= C_{k-1} \exp(hA_k) \\ \alpha_k &= \|C_k^*\| \\ C_k &= \alpha_k^{-1} C_k^* \end{aligned} \right\} k = 1 \ldots \ldots N \qquad (59)$$

and finally

$$B = \exp\left(\sum_{k=1}^{N} \log(\alpha_k)\right) C_N \qquad (60)$$

4.1.2
Evaluation of the monodromy matrix through newmark time integration
Let us again assume the system (45) is time invariant between consecutive discrete time instants t_k and t_{k+1}. If we make use of the approximation formulas for the Newmark method

$$\begin{aligned} \dot{y}_{k+1} &= \dot{y}_k + (1 - \gamma)h\ddot{y}_k + \gamma h\ddot{y}_{k+1} \\ y_{k+1} &= y_k + h\dot{y}_k + h^2(\tfrac{1}{2} - \beta)\ddot{y}_k + h^2\beta\ddot{y}_{k+1} \end{aligned} \qquad (61)$$

and express the equations of linearized dynamic equilibrium at times t_k and t_{k+1}

$$\begin{aligned} M\ddot{y}_k &= -C_k\dot{y}_k - K_k y_k \\ M\ddot{y}_{k+1} &= -C_{k+1}\dot{y}_{k+1} - K_{k+1}y_{k+1} \end{aligned} \qquad (62)$$

the combination of (61) and (62) and pre-multiplication by the mass matrix yields

$$\begin{aligned} My_{k+1} &= My_k + hM\dot{y}_k + (\tfrac{1}{2} - \beta)h^2\left[-C_k\dot{y}_k - K_k y_k\right] \\ &\quad + \beta h^2\left[-C_{k+1}\dot{y}_{k+1} - K_{k+1}y_{k+1}\right] \\ M\dot{y}_{k+1} &= M\dot{y}_k + h(1 - \gamma)\left[-C_k\dot{y}_k - K_k y_k\right] \\ &\quad + \gamma h\left[-C_{k+1}\dot{y}_{k+1} - K_{k+1}y_{k+1}\right] \end{aligned} \qquad (63)$$

Equation (63) can be put into the discrete matrix form

$$x_{k+1} = D_k x_k \qquad (64)$$

with the transition matrix

$$D_k = H_1^{-1}H_0 \qquad (65)$$

Matrices H_1 and H_0 are computed in terms of the mass, damping and stiffness matrices as follows:

$$H_1 = \begin{bmatrix} M + \beta h^2 K_{k+1} & \beta h^2 C_{k+1} \\ \gamma h K_{k+1} & M + \gamma h C_{k+1} \end{bmatrix} \qquad (66)$$

$$H_0 = \begin{bmatrix} M - (\frac{1}{2} - \beta)h^2 K_{k+1} & hM - (\frac{1}{2} - \beta)h^2 C_{k+1} \\ -(1 - \gamma)h K_{k+1} & M - (1 - \gamma)h C_{k+1} \end{bmatrix} \qquad (67)$$

Note that, in fact, the transition matrix D_k can be seen as another form of approximation to the matrix exponential $\exp(hA_k)$.

Having obtained the expression of the transition matrix between any two consecutive instants, the monodromy matrix is computed by performing the products of all of them. To this end, we use the algorithm with normalization of partial products at each step. The algorithm parameters are set to $\gamma = \frac{1}{2}$ and $\beta = \frac{1}{4}$ so that the scheme is unconditionally stable and no amplitude error is introduced.

Numerical experiments have shown that in order to D_k approximate correctly the matrix exponential $\exp(hA_k)$, the time step should be less than $1/10$ of the minimum period of the system

$$h < \frac{T_{\min}}{10} = \frac{2\pi}{10\omega_{\max}} \qquad (68)$$

Below this threshold, $D_k \rightarrow \exp(hA_k)$ quadratically with h. This relation gives us a means to estimate an appropriate value of h for stability analysis.

We should mention, however, that numerical experiments have shown when using larger time steps that the computed Floquet multipliers are upper estimates to exact values. Therefore the algorithm gives conservative results from the point of view of stability assessment, a property of great value in practice.

5
Numerical results

In order to assess the performance of the method, we next present three application examples: a Duffing oscillator, a clamped beam with a friction damper and a shallow hanging cable with an oscillating support.

5.1
Duffing oscillator

Duffing's equation is written as follows

$$\ddot{x} + c\dot{x} + kx + k_{nl}x^3 = F\cos(\omega t) \qquad (69)$$

It is representative of a large class of nonlinear problems. Consider for instance a nonlinear pendulum where the linear assumption $(\sin(x) \approx x)$ is replaced by the third degree approximation $(\sin(x) \approx x - \frac{1}{6}x^3)$. The interest in Duffing's equation resides mainly in the fact that it can produce a large number of solution types and therefore has been thoroughly described in the literature [32–35].

The response behavior depends essentially on the magnitude and the sign of the nonlinear term $k_{nl}x^3$. The proposed method has been tested in the following case

$$\ddot{x} + 0.02\dot{x} + x + k_{nl}x^3 = \cos(\omega t) \qquad (70)$$

for excitations in the range 0.02 Hz–0.7 Hz. The linear eigenfrequency is $\omega_0 = 0.1592$ Hz. The sub-harmonic resonance frequency is located near $\frac{1}{3}\omega_0 = 0.053$ Hz.

The multi-harmonic balance method has been applied for the following parameters set: 1024 sampling points, analysis period equal to 3 excitation periods and 15 harmonics retained.

In order to investigate the global response behavior, various simulations have been performed for different values of the k_{nl} parameter. Figure 2 displays the curves of displacement amplitude versus frequency obtained for different values of k_{nl}. They agree with the theoretical predictions [32, 34] and coincide with the results obtained by Crooijmans [36]. We see that the curves are bent to the right for positive values of k_{nl} and to the left for negative values. In all cases where $k_{nl} < 0$ the computation has to be organized in two steps due to the fact that the nonlinear dynamics path becomes discontinuous. The number of computation points for tracing these curves was comprised between 100 and 500 and the mean number of iterations at each point was equal to 3.

All curves traced for $(k_{nl} \neq 0)$ present a disturbance at a frequency very close to $\frac{1}{3}\omega_0$ corresponding to sub-harmonic resonance. The sub-harmonic response exhibits a difference in behavior depending on the magnitude and sign of the nonlinear parameter k_{nl}. This can be observed by zooming on the previous diagram about $\frac{1}{3}\omega_0$ (see Fig. 3).

Next, we analyze more specifically the results obtained for the case $k_{nl} = 0.04$. The resonance curve presents a deflection to the right and the sub-harmonic resonance occurs at 0.055 Hz. Observing the response in the phase plane explains the nature of the sub-harmonic resonance (see Fig. 4). For a frequency of 0.4836 Hz (which corresponds to maximum amplitude) we get a diagram with one loop per cycle. For a frequency of 0.055 Hz (which corresponds to the sub-harmonic resonance frequency) the
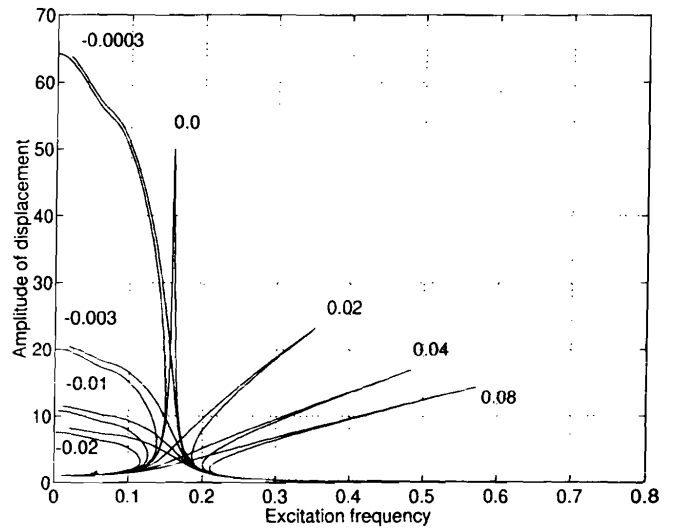

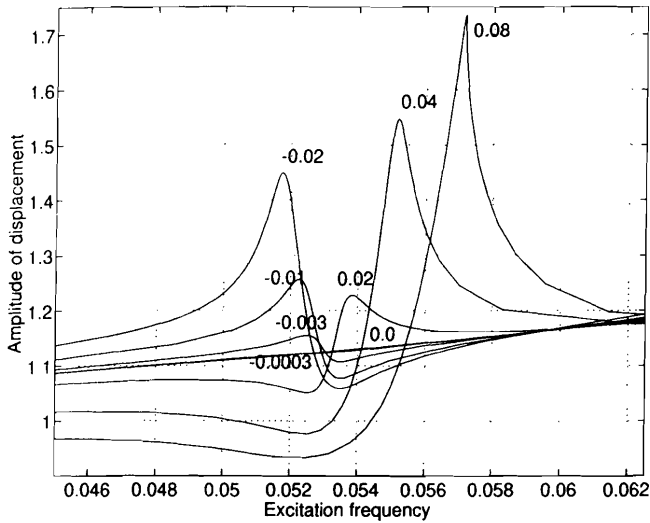Fig. 2. Resonance curves of the Duffing oscillator for different values of the parameter k_{nl}.

Fig. 3. Zoom over the resonance curves of the Duffing oscillator for different values of the parameter k_{nl}.
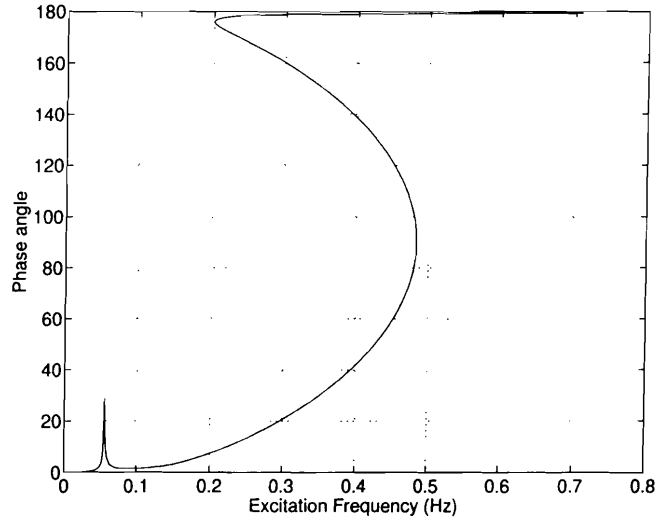

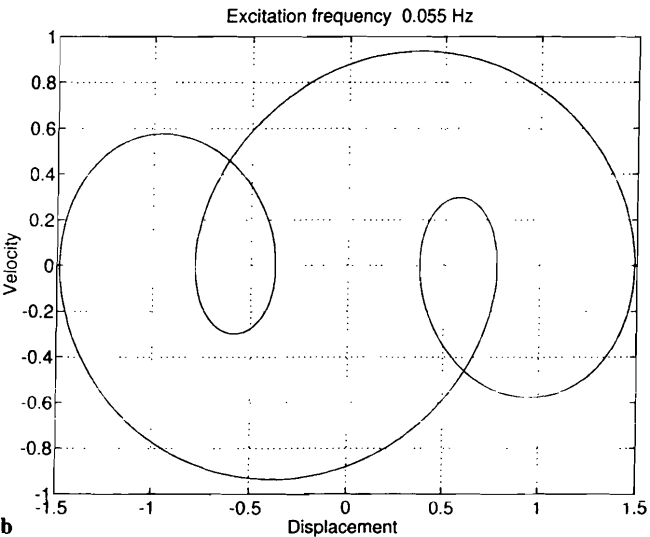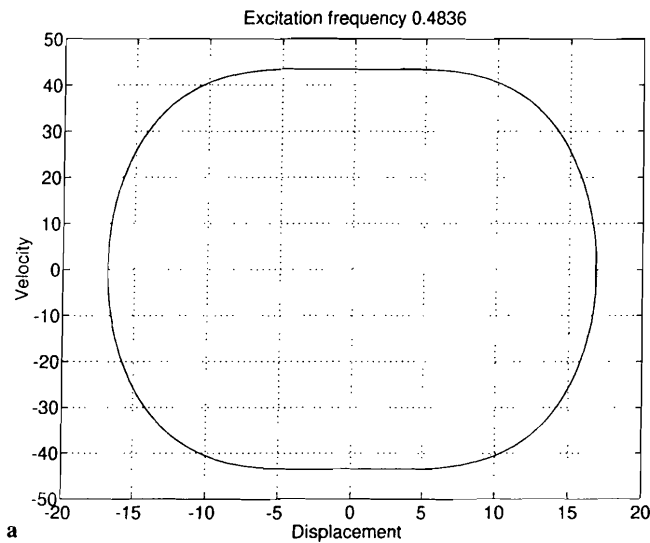**Fig. 5.** Plot of phase angle versus frequency for the Duffing oscillator with $k_{nl} = 0.04$.

Fig. 4a,b. Phase diagrams for the Duffing oscillator with $k_{nl} = 0.04$. **a** one loop per cycle response at 0.4836 Hz. **b** three loops per cycle response at 0.0055 Hz.

diagram obtained presents 3 loops per cycle. Finally, the plot of phase angle versus frequency (Fig. 5) provides the same type of information with a peak located at the subharmonic resonance frequency.

Finally, we investigate the stability of the computed response by the methods of matrix exponentiation and Newmark time integration. Figure 7 displays the maximum norm of the Floquet coefficients for both methods and for different numbers of FFT sampling points. We see on Fig. 7 that both methods converge to the same solution. We note however that for a small number of points the Floquet multipliers predicted by the Newmark algorithm are greater than those predicted by matrix exponentiation.

Numerical experiments have shown that convergence to the characteristic multipliers computed by the Newmark algorithm occurs by upper bounds (this can be related to the fact that the integration error produces an artificial elongation in the computed period). This behavior indicates that the results are conservative in the sense that they predict greater level of instability.

Finally, Fig. 6 plots the zones of instability in the response.

5.2
Clamped beam with dry-friction damper

The problem of determining the periodic response of a friction-damped dynamic system has been treated by many authors [37, 9, 7, 39, 39, 15]. Here we have analyzed the response of a clamped beam with a dry-friction damper located at nearly one-fourth of its length and submitted to a periodic excitation at its tip (see Fig. 8). Numerical results have been compared to experimental data for a broad frequency range.

The material and geometrical properties of the beam are: Young modulus $E = 2.0 \times 10^{11}$ Pa, Poisson ratio $v - 0.3$, mass density $\rho = 8125$ kg/m^3, cross-sectional area $A = 4.64 \times 10^{-4}$ m^2 and inertia $I = 1.312 \times 10^{-7}$ m^4. Two lumped inertias are placed over the beam. The first one is located at the connection with the friction damper: its mass equals $m_1 = 2$ kg and its inertia
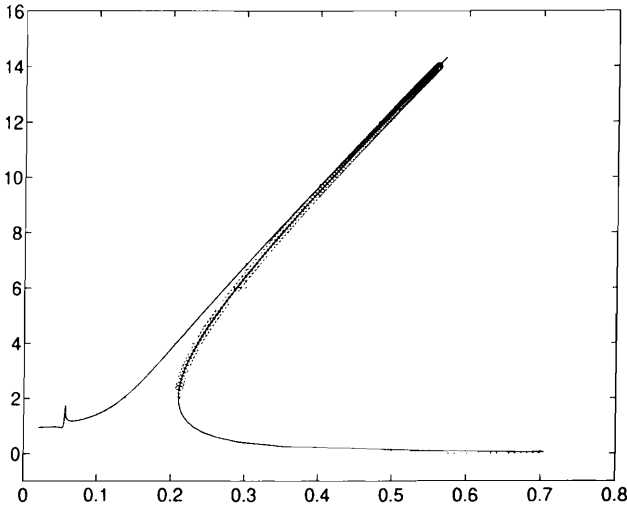
Fig. 6. Duffing oscillator : zone of response instability (circles) for $k_{nl} = 0.04$

$J_1 = 0.85 \times 10^{-4}$ kg m^2. The second one is located at the beam tip, with mass $m_2 = 0.326$ kg. The dry-friction damper has a spring constant $k = 2.4 \times 10^{-7}$ N/m, a Coulomb friction coefficient $\mu = 0.66$ and the compression force is constant and equal to $N = 372.8$ N. Three different cases have been analyzed for three different values of load amplitudes: 0.938 N, 29.063 N and 38.348 N.

The beam has been modeled by using three Bernoulli beam finite elements. Structural damping has been determined considering the damper locked (no sliding was allowed). Rayleigh damping has been assumed in the form $\alpha M + \delta K$ with constants $\alpha = 1.039 \times 10^{-4}$ and $\delta = 3.741$. The latter values correspond to a structural damping $\epsilon_1 = 2.37$ per cent for the first mode at frequency 35.2 Hz.

The number of FFT points is equal to 2048, the period of analysis is 4 times the excitation period and the number of harmonics is equal to 12.

Figure 9 displays the maximum displacement amplitude at the tip of the beam in terms of the excitation frequency for the three values of force amplitude. These results are compared to those obtained experimentally [40], showing a good agreement. For small values of excitation amplitude the friction damper is locked and therefore the system exhibits almost linear behavior. For increasing force values the friction damper unlocks and begins to damp out energy from the system. At the same time, the frequency at the response peak is shifted down from 35.2 to 26 Hz. Figure 10 presents a plot in the complex plane of all Floquet coefficients in the frequency range of analysis and for the intermediate value of excitation force ($F_{exc} = 29.063$ N). The computations were performed using the exponential matrix method. All Floquet coefficients lie inside the stability zone limited by the unit circle.

The computation of Floquet coefficients based on the Newmark approximation is considered next. We can observe on Fig. 11 that some differences occur between Newmark's and truncated power series results when using 1024 sampling points. However, when increasing the number of points to 2048 both methods agree almost completely.
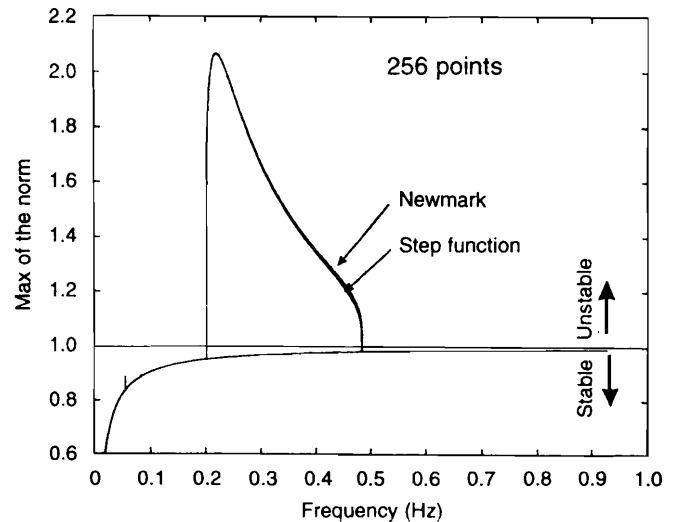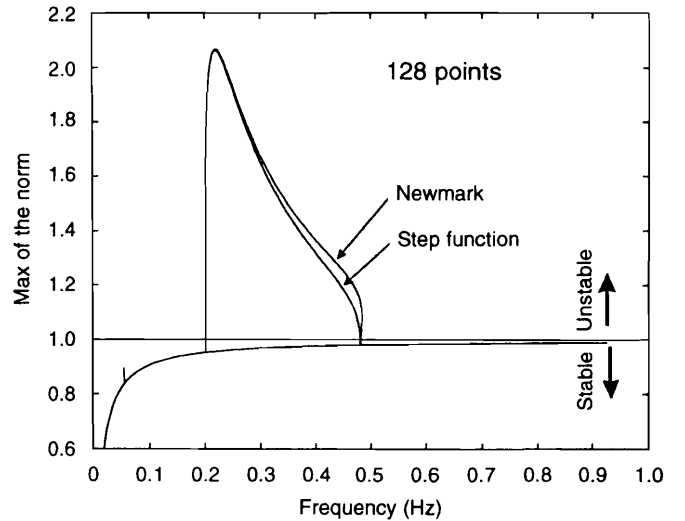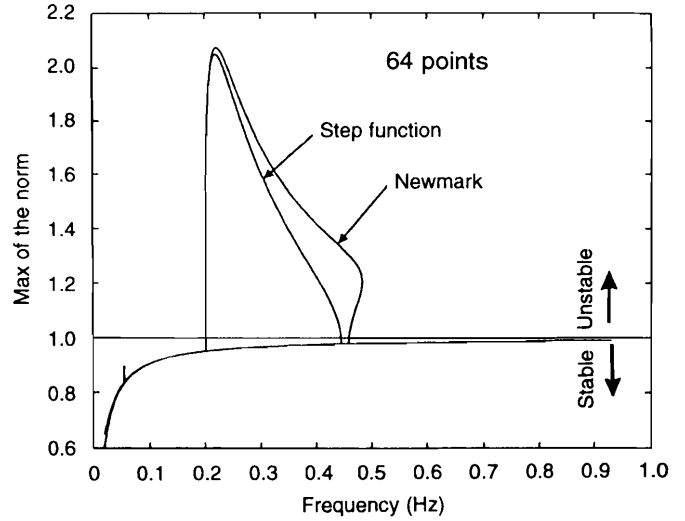

Fig. 7. Duffing oscillator: norm of Floquet coefficients versus frequency for different number of integration points (64, 128, 256 points)

Again, we see that the Floquet multipliers predicted by Newmark's approximation are greater than by matrix exponentiation and that upper bound convergence to the
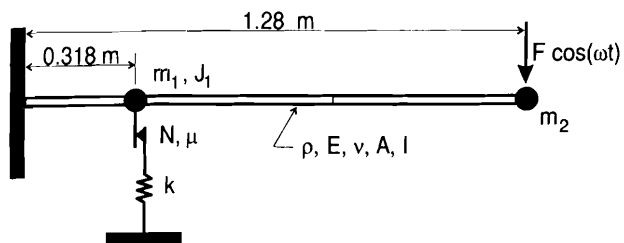
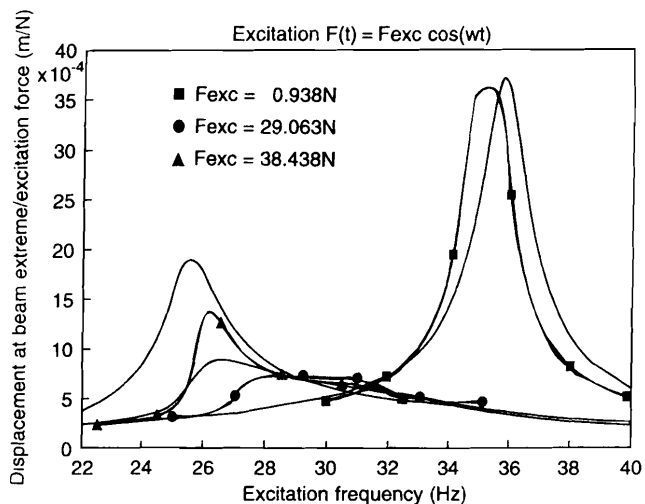Fig. 8. Clamped beam with dry-friction damper

Fig. 9. Clamped beam with dry-friction damper: maximum displacement amplitude versus frequency at the beam tip. Thick lines: experimental results. Thin lines: results of numerical computations.
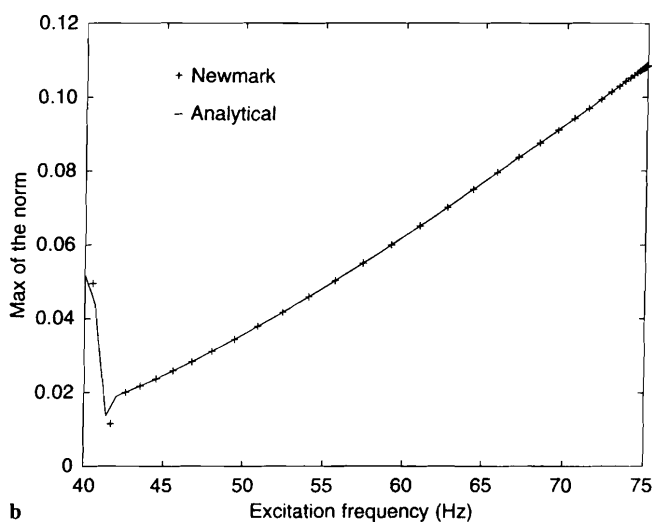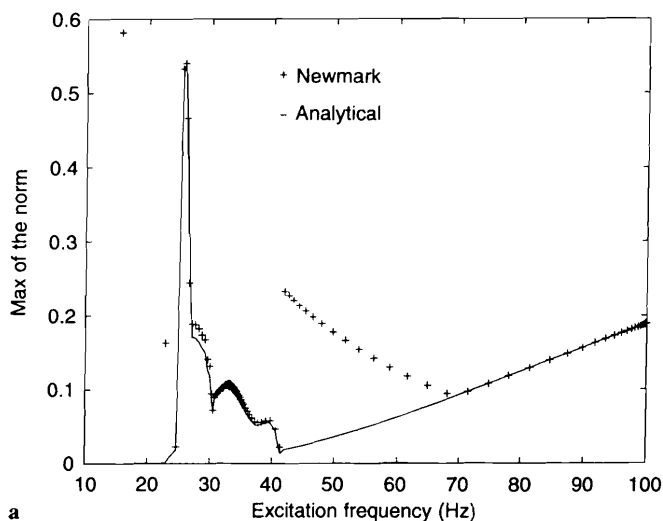

Fig. 10. Clamped beam with dry-friction damper : complex plane plot of the Floquet coefficients

Fig. 11a,b. Clamped beam with dry-friction damper: norm of Floquet coefficients versus frequency. a 1024 sampling points. b 2048 sampling points.
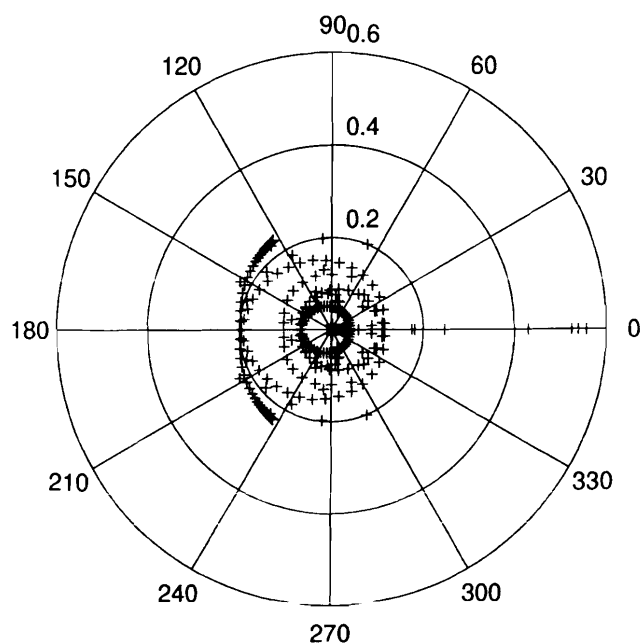
final values of the characteristic multipliers is thus obtained.

5.3
Shallow hanging cable

The last example consists into computing the harmonic response of a hanging cable submitted to imposed periodic displacement at one edge, the other edge being fixed (Fig. 12). This parametric excitation problem has been considered previously by several authors [41–43].

The displacements of the cable are denoted by $u(s, t)$, where s is the arc-length coordinate and t the time. The axial strain in the cable $\varepsilon(s)$ can be expressed in the form [41]

$$\varepsilon = \frac{F}{EA} + u_1' - \kappa u_2$$

$$+ \frac{1}{2}\left[\left(u_1' - \kappa u_2\right)^2 + \left(u_2' + \kappa u_1\right)^2 + \left(u_3'\right)^2\right] \tag{71}$$

where $u' = \frac{\partial u}{\partial s}$ and where E is the Young modulus, A is the cable normal cross-section, $F(s)$ represents the tension

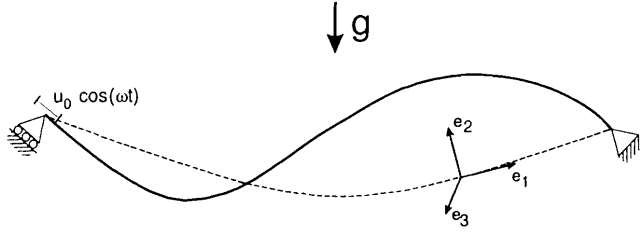**Fig. 12.** Geometric description of the hanging cable

Table 1. Natural frequencies of a shallow hanging cable

Description of mode shape	Natural frequency (Hz) [46]
Shallow parabolic sag	0
Out-of-plane mode	$\frac{i}{2\ell}\left(\frac{E}{\rho}\right)^{\frac{1}{2}}$
In-plane mode (skew-symmetric)	$\frac{i}{\ell}\left(\frac{E}{\rho}\right)^{\frac{1}{2}}$
In-plane mode (symmetric)	$\frac{\lambda_i}{2\ell}\left(\frac{E}{\rho}\right)^{\frac{1}{2}}$

into the cable in the equilibrium configuration and $\kappa(s)$ the curvature. The kinetic energy $\mathcal{K}$ and strain energy $\mathcal{V}$ of the cable system are given by

$$\mathcal{K} = \int_0^\ell \frac{1}{2}\rho\dot{\mathbf{u}} \cdot \dot{\mathbf{u}}\, ds \tag{72}$$

$$\mathcal{V} = \mathcal{V}_0 + \int_0^\ell F\varepsilon + \frac{1}{2}EA\varepsilon^2$$
$$- \rho g[u_1 \sin\theta + u_2 \cos\theta]\, ds \tag{73}$$

where ρ is the mass density, g is the gravity acceleration and θ is the angle between $\mathbf{e}_1$ and the horizontal and ℓ is the length of the cable.

The boundary conditions are

$$\mathbf{u}(0, t) = \mathbf{u}_0 \cos(\omega t) \tag{74}$$

$$\mathbf{u}(\ell, t) = \mathbf{0} \tag{75}$$

where $\mathbf{u}_0$ is the amplitude of imposed displacements at the end. An approximate solution is computed by a six terms expansion using the Rayleigh–Ritz method

$$\mathbf{u}(s, t) = \mathbf{u}_0 \cos(\omega t)\left(1 - \frac{s}{\ell}\right) + \begin{Bmatrix} q_1 \\ q_2 \\ q_3 \end{Bmatrix}\sin\left(\frac{\pi s}{\ell}\right)$$

$$+ \begin{Bmatrix} q_4 \\ q_5 \\ q_6 \end{Bmatrix}\sin\left(\frac{2\pi s}{\ell}\right) \tag{76}$$

where $\mathbf{q} = [q_1 q_2 \ldots q_6]$ are the new generalized coordinates. The static deformation of the cable has been approximated by a parabolic curve.

The system behaviour is governed by Lagrange equations of motion

$$\frac{d}{dt}\left(\frac{\partial \mathscr{L}}{\partial \dot{\mathbf{q}}}\right) - \frac{\partial \mathscr{L}}{\partial \mathbf{q}} = \mathbf{0} \tag{77}$$

where $\mathscr{L}(\mathbf{q}, \dot{\mathbf{q}}) = \mathcal{K} - \mathcal{V}$ is the system Lagrangian.

The equations of motion (77) and the tangent mass, damping and stiffness matrices have been computed through symbolic differentiation using the Maple software [44]. The Fortran computer code was also generated in this way. Further details on the model are given in reference [45].

The motion equations contain both quadratic and cubic terms, inducing thus sub-harmonics ($\frac{1}{2^n}$, $\frac{1}{3^n}$, $n = 1, 2, 3 \ldots$) in the response. They are responsible for the complex response pattern due to coupling between in-plane and out-

of-plane modes. The free vibration frequencies and mode shapes are listed in Table 1 ($\lambda_1 = 1$, $\lambda_2 = 3, \ldots$ in this problem).

The system analyzed corresponds to a one stay of the Ben-Ahin bridge which has been previously studied using finite elements [21]. The system data are summarized as follows: length 110.505 m, mass density 62.841 kg/m, Young modulus 210 Gpa, initial sag at mid-length $y_0 = 0.2$ m, cross-section 0.00826 m^2, tension 4895190 N.

The set of parameters used to compute the response by the MHB method are: initial excitation frequency 0.1 Hz, final excitation frequency 5 Hz, 256 sampling points, time sampling over 3 excitation periods, 16 number of harmonics and average number of iterations set to 3.

The forced response of the hanging cable has been studied for various forms of excitation and damping. In this work, we present results for the case with axial excitation at the moving end ($u_0 = 0.05$ m) and zero damping. Figure 13 displays the computed peak-to-peak amplitudes of motion in terms of excitation frequency. We can observe the presence of sub-harmonics and Duffing-like behavior. The first resonance occurs at $\frac{1}{3}\omega_1$ and results from the presence of cubic non-linearities. The second one corresponds to $\frac{1}{2}\omega_1$ and results from the presence of quadratic non-linearities. The third resonance corresponds to ω_1 but also to $\frac{1}{2}\omega_2$. Therefore, for this frequency a dynamic bifurcation exists. One branch has a mode
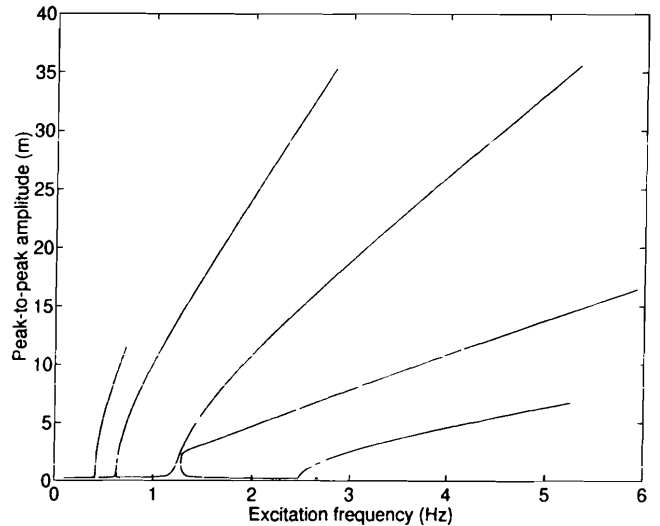

Fig. 13. Hanging cable: peak-to-peak amplitude versus excitation frequency
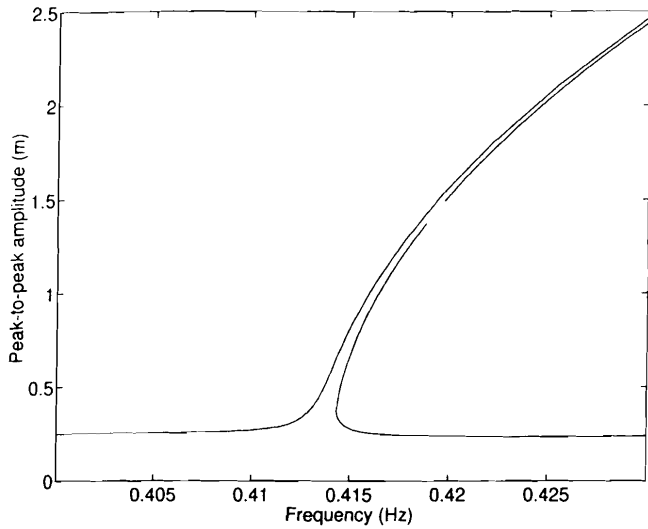
Fig. 14. Hanging cable: peak-to-peak amplitude in 0–0.5 Hz frequency range
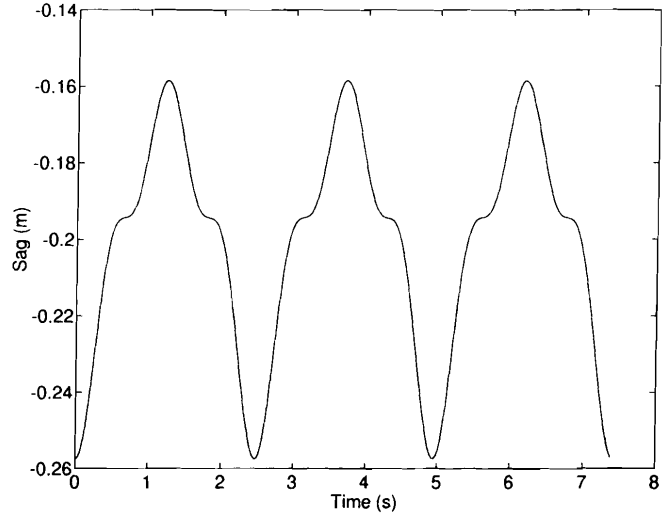

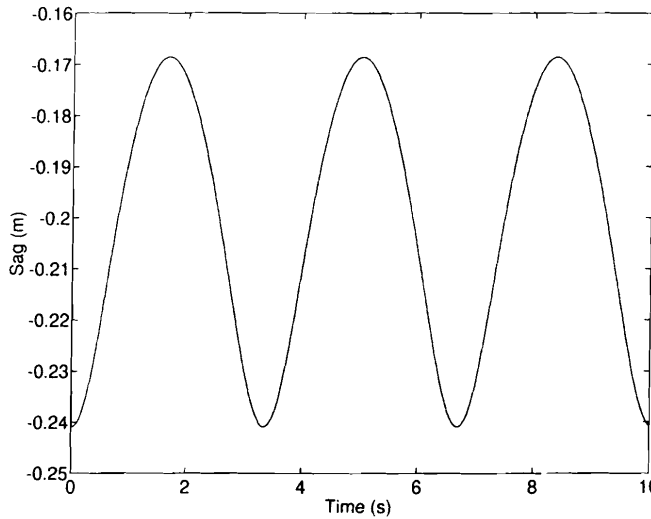**Fig. 16.** Hanging cable: sag at mid-length for excitation frequency = 0.4 Hz

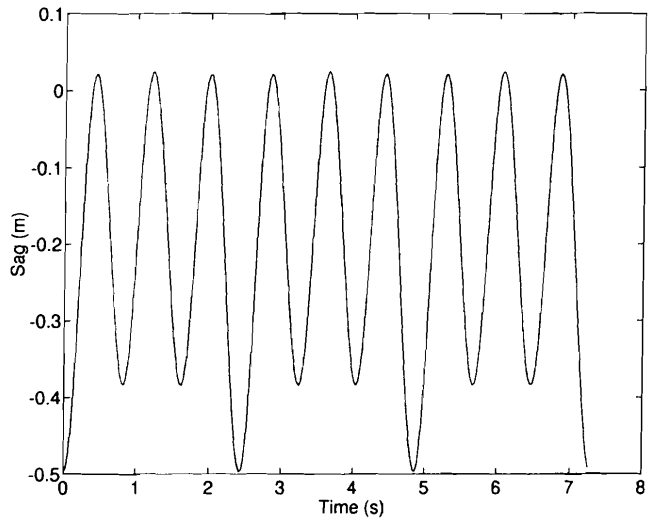**Fig. 15.** Hanging cable: sag at mid-length for excitation frequency = 0.3 Hz

Fig. 17. Hanging cable: sag at mid-length for excitation frequency = 0.4138 Hz

shape corresponding to the first eigenmode, the second one has a mode shape corresponding to the second eigenmode. The fourth resonance occurs ω_2.

Two zones have been analyzed with greater detail. The first one is the zone around the first resonance (0.41 Hz) and the second is located around the third resonance peak (1.24 Hz).

Figure 14 provides a plot of the first resonance located at $\frac{1}{3}\omega_1$. At lower frequency (Fig. 15) the motion in the middle of the cable is harmonic and the period of the response corresponds to the period of the excitation (computations have been performed on a period corresponding to three periods of the excitation). When increasing the excitation frequency (Fig. 16) wave reflections occur and produce stops into the cable motion. Figure 17 shows that when the excitation is equal to $\frac{1}{3}\omega_1$, the stops of Fig. 16 have grown into a sinusoidal response with frequency equal to ω_1. Figure 17 is also of interest because

this is the first time that the cable motion crosses the X axis. This is a very dangerous resonance in practice since it develops at a very low excitation frequency. By still increasing the excitation frequency one also increases the response amplitude but the shape of motion does no longer change.

The response computed around 1.24 Hz is of great interest since the system exhibits a dynamic bifurcation in that zone. By making a frequency sweep we get the curve of (Fig. 18). At the left end, when the excitation frequency equals 1.3024 Hz, the motion corresponds to the first eigenmode (Fig. 19). When increasing slowly the excitation frequency one observes that two "partially fixed points" are generated. These two points move to the X axis to finally merge into one nodal point at frequency 1.4399 Hz. Therefore we observe that on a very narrow band of excitation frequency the system response switches from the first mode to the second one (Figs. 19–22).
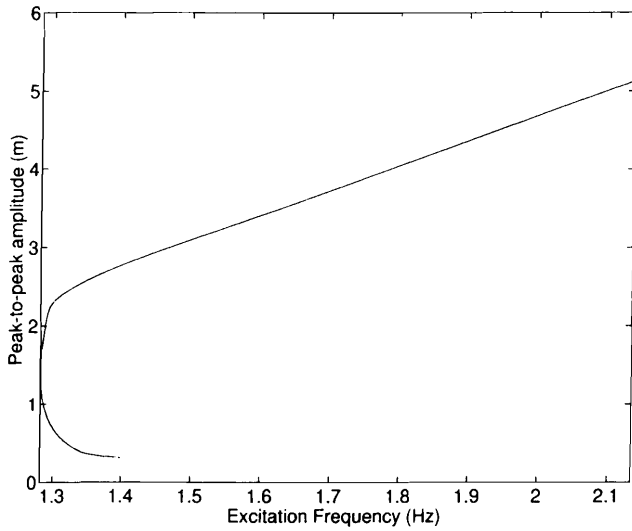
Fig. 18. Hanging cable: peak-to-peak response amplitude in frequency range 1.3–2.1 Hz
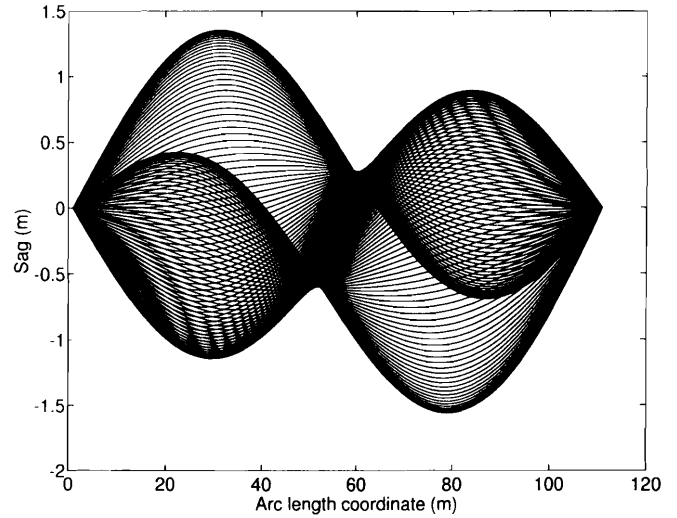

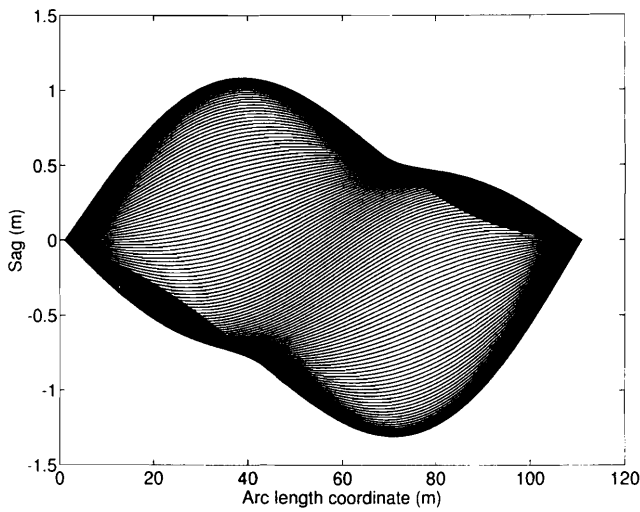**Fig. 21.** Hanging cable: sag evolution with time versus cable span for excitation frequency = 1.345 Hz

Fig. 19. Hanging cable: sag evolution with time versus cable span for excitation frequency = 1.3024 Hz
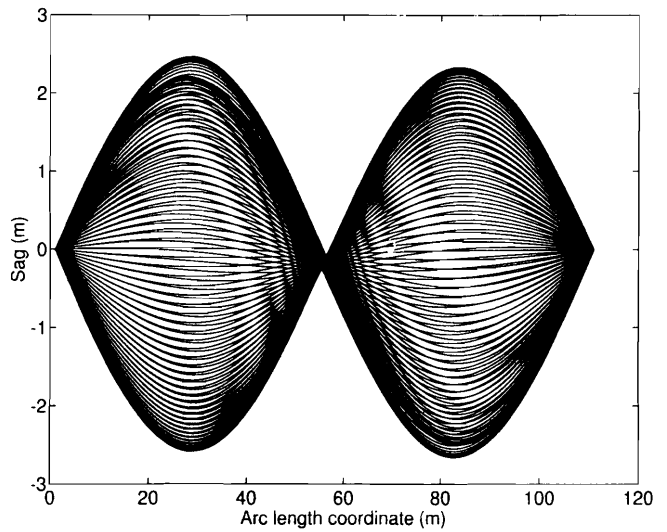

Fig. 22. Hanging cable: sag evolution with time versus cable span for excitation frequency = 1.4399 Hz
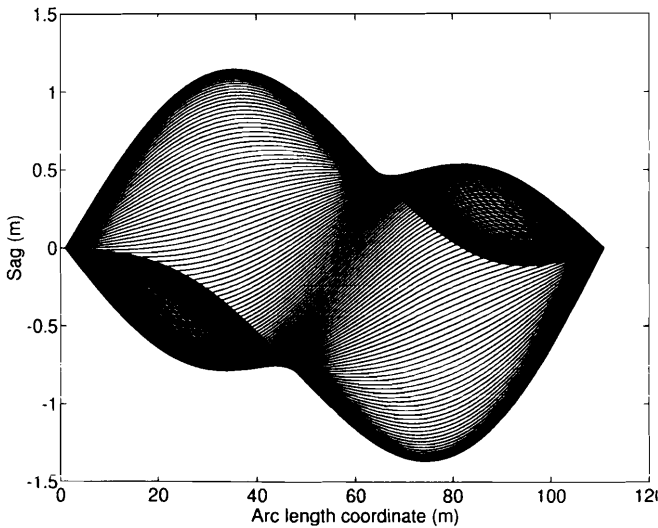
6
Concluding remarks

A multiharmonic method to solve general nonlinear dynamic systems submitted to periodic external forces has been developed. The method is based on a systematic use of the FFT algorithm to transfer the motion equations from the time domain to the frequency domain and vice versa. The Jacobian matrix of the resulting system of nonlinear algebraic equations is exactly evaluated, reaching quadratic convergence rate in the iterative solution.

A Crisfield type continuation method has been implemented to trace the nonlinear dynamic solution path. Again, the FFT is used to evaluate the additional derivatives required to evaluate the matrix of coefficients.

The stability of the computed periodic solutions has been investigated by a Floquet method. Two approaches for computing the monodromy matrix have been tested: a first one in which matrix exponentials are evaluated by

Fig. 20. Hanging cable: sag evolution with time versus cable span for excitation frequency = 1.31 Hz

truncated Taylor series and a second one based on Newmark's time integration formula. The latter approach yields conservative results about system stability in the sense that numerical experiments showed that predicted Floquet multipliers converge by upper bounds to the true values.

Several application examples of application have been described to illustrate the power of the proposed approach. In particular, an example involving cable vibrations in a stay of cable-suspended bridge has been presented in detail.

References

1. **Urabe M** (1965) Galerkin's procedure for nonlinear periodic systems. Arch. Mech. Anal., 20(2):120-152
2. **Urabe M, Reiter A** (1966) Numerical computation of nonlinear forced oscillations by galerkin's procedure. J. Math. Anal. Applic., 14:107-140
3. **Lau SL, Cheung YK** (1981) Amplitude incremental variational principle for nonlinear vibration of elastic systems. ASME J. Appl. Mech., 28:959-964
4. **Lau SL, Cheung YK, Wu SY** (1982) A variable parameter incrementation method for dynamic instability of linear and nonlinear elastic systems. J. Appl. Mech., 49:849-853, December
5. **Lau SL, Cheung YK, Wu SY** (1983) Incremental harmonic balance with multiple time scales for aperiodic vibrations of nonlinear systems. J. Appl. Mech., 50:871-876, December
6. **Lau SL, Zhang WS** (1992) Nonlinear vibrations of piecewise-linear systems by incremental harmonic balance method. ME J. Appl. Mech., 59:153-160
7. **Pierre C, Ferri AA, Dowell EH** (1985) Multi-harmonic analysis of dry friction damped systems. J. Appl. Mech. 52:958-964
8. **Pierre C, Dowell EH** (1985) A study of dynamic instability of plates by an extended incremental harmonic balance method. ASME J. Appl. Mech., 52:993-997
9. **Aldo F Ferri** (1985) The Dynamics of Dry Damped Systems. PhD thesis, Princeton University, September. A dissertation presented to the faculty of Princeton University in candidacy for the degree of doctor of philosophy
10. **Ling FH, Wu XX** (1987) Fast galerkin method and its application to determine periodic solutions of nonlinear oscillators. Int. J. Nonlinear Mech. 22:89-98
11. **Cameron TM, Griffin JH** (1989) An alternating frequency/time domain method for calculating the steady-state response of nonlinear dynamic system. J. Appl. Mech. 56:149-154, March
12. **Kanarachos AE, Spentzas CN** (1992) A galerkin method for the steady state analysis of harmonically excited non-linear systems. Mechanisms and Machine Theory, 27:661-671
13. **Kim YB, Noah ST** (1991) Stability and bifurcation analysis of oscillators with piecewise linear characteristics - a general approach. ASME J. Appl. Mech., 58:545-553
14. **Lewandowski R** (1992) Nonlinear, steady-state vibration of structures by harmonic balance/finite element method. Comput. Struct., 44(1/2):287-296
15. **Cardona A, Coune T, Lerusse A, Géradin** (1991) A multi-harmonic method for nonlinear vibration analysis. Intl. J. Numer. Meth. in Eng., 37:1593-1608
16. **Lerusse A, Géradin M** (1994) Multi-harmonic balance method applied to nonlinear structures. Technical Report VA-140, LTAS, April
17. **Crisfield MA** (1991) Non-Linear Finite Element Analysis of Solids and Structures. John Wiley
18. **Cardona A, Huespa AE** Continuation methods for tracing the equilibrium path in flexible mechanism analysis. Technical

report, Grupo de Technoloía Mecánica - INTEC, 1996. To appear in Engineering Computations
19. **Hsu CS** (1974) On approximating a general linear periodic system. J. Math. Anal. Applic., 45:234-251
20. **Friedmann P, Hammond CE, Woo TH** (1977) Efficient numerical treatment of periodic systems with application to stability problems. Intl. J. Numer. Meth. in Eng., 11:1117-1136
21. **Lilien JL, Pinto Da Costa A** (1994) Vibration amplitudes caused by parametric excitation of cable stayed structures. J. Sound & Vibration, 174(1):69-90
22. **Brigham EO** (1974) The Fast Fourier Transform. Prentice Hall Inc.
23. **Felippa CA** (1988) Lecture notes on solution of nonlinear structural equations. Technical Report CU-CSSC-88-06, University of Colorado Boulder, May
24. **Fried I** (1984) Orthogonal trajectory accession to the nonlinear equilibrium curve. Comput. Meth. Appl. Mech. Eng., 47:283-297
25. **Cardona A, Huespe AE** (1997) Evaluation of simple bifurcation points and post-critical path in large finite rotation problems. Technical report, Grupo de Technología Mecánica - INTEC. Submitted to J. Multibody Systems Dynamics
26. **Keller HB** (1983) The Bordering algorithm and path following near singular points of higher nullity. SIAM J. Sci. Stat. Comput., 4:575-582
27. **Crisfield MA** (1981) A fast incremental/iterative solution procedure that handles snap-through. J. Comp. and Struct., 13:55-62
28. **Weyh B, Kostyra H** (1991) Direct floquet method for stability limits determination - i: Theory. Mech. Mach. Theory, 26(2):123-131
29. **Lerusse A, Géradin M** (1994) Determination of solution stability by a floquet method. Technical Report VA-149, LTAS, October
30. **Moler C, Van Loan C** (1978) Nineteen dubious ways to compute the exponential of matrix. SIAM Review, 20(4):801-836, October
31. **Golub GH, Van Loan CF** (1991) Matrix Computations. The Johns Hopkins University Press
32. **Nayfeh AH, Mook DT** (1979) Nonlinear Oscillations. Wiley
33. **Hagedorn P** (1982) Non-linear Oscillations. Oxford Engineering Science Series
34. **Jordan DW, Smith P** (1987) Nonlinear Ordinary Differential Equations. Oxford applied mathematics and computing science series
35. **Rao JS** (1989) Advanced Theory of Vibration. John Wiley & Sons
36. **Crooijmans MTM** (1987) On the computations of stationary deterministic behaviour of non-linear dynamic systems to rotor bearing structures. PhD thesis, Eindhoven University of Thechnology
37. **Den Hartog** (1931) Forced vibration with combined coulomb and viscous frictions. Trans ASME, APM-53(9):107-115
38. **Klepp HJ** (1991) Steady-state and irregular motion of a system with friction under harmonic excitation. Mech. Struct. & Mach., 19(3):327-356
39. **Wang JH, Chen WK** (1992) Investigation of the vibration of a blade with friction damper by hbm. In int. Gas Turbine Congress, Pages 1-4, Cologne, June 1992. ASME
40. **Berthillier M** (1992) Private communication. Technical report, SNECMA, July 1992
41. **Perkins NC** (1992) Modal interactions in the non-linear response of elastic cables under parametric/external excitation. Int. J. Nonlinear Mech., 2:233-250
42. **Lilien JL** (1983) Contraintes et conséquences électromécaniques liées au passage d'une intensité de courant dans les structures en câbles. PhD thesis, Université de Liège. thèse de doctorat en Sciences Appliquées.

43. Valette C, Cuesta C (1993) Mécanique de la corde vibrante. Traité des Nouvelles Technologies serie Mécanique. Hermes

44. Char BW, Geddes KG, Gonnet GH, Leing BL, Monagan MB, Watt SM (1992) First Leaves: A tutorial introduction to Maple V. Springer-Verlag

45. Lerusse A (1995) Application of the multi-harmonic balance method to cable stayed structure. Technical Report VA-159, LTAS, April

46. Blevins RD (1979) Formulas for natural frequency and mode shape. Van Nostrand Reinhold Comp.

47. Bar-Yoseph PZ, Fisher D, Gottlieb O (1996) Spectral Element Methods for Nonlinear Temporal Dynamic Systems. Comput. Mech. 18:302–313